

## Electron capture and excitation in proton- $\text{Na}_{20}$ collisions at low velocities

M. F. Politis

*GPS, Université de Paris VII, 2 place Jussieu, 75251 Paris, France*

P. A. Hervieux, J. Hanssen, and M. E. Madjet

*LPMC, Institut de Physique, Technopôle 2000, 57078 Metz, France*

F. Martín

*Departamento de Química, C-9, Universidad Autónoma de Madrid, 28049 Madrid, Spain*

(Received 19 December 1997)

We present a many-electron theoretical study of electron capture and excitation in collisions of  $\text{H}^+$  with  $\text{Na}_{20}$  clusters for impact energies 40–500 eV. The collision is treated semiclassically using the independent-electron model, and the cluster is described in the framework of the Kohn-Sham formalism with a local-density approximation which includes exchange, correlation, and a self-interaction correction. We have found that capture cross sections are  $\sim(2-5)\times 10^{-14}$  cm<sup>2</sup> and dominate in the above energy range. In contrast with ion-atom collisions, excitation cross sections are comparable to the former, and multiple processes such as capture excitation cannot be neglected at low velocities. From the analysis of the vacancies originated in the collision, we have evaluated the energy deposited in the cluster, which is an essential parameter in the study of cluster fragmentation. [S1050-2947(98)08406-6]

PACS number(s): 36.40.Sx, 34.70.+e

### I. INTRODUCTION

Cluster research is a rapidly growing field in which many branches of physics and chemistry are involved [1–3]. In the early stages of this field, a crucial problem was to determine the structure and static properties of clusters. But, in the last few years, these investigations are turning to the study of dynamical aspects that may probe their properties and may lead to the discovery of new interesting phenomena and applications [4–11]. At present, free clusters of a well defined number of alkali-metal atoms are experimentally available [3], which opens up the way for a *clean* and *meaningful* study of their interactions with atoms, molecules, and surfaces. As an example, recent experimental work [12,13] has shown that low energy collisions of metal clusters with highly charged ions is an efficient way to produce positively charged clusters. An interesting application of this technique is the formation of clusters with critical charge-size ratios which lead to fragmentation. There are several mechanisms that can lead to the formation of positively charged clusters by ion impact: single and multiple capture, single and multiple ionization, capture ionization, capture excitation, etc. All these processes have been extensively studied in ion-atom collisions, but very little is known about them in ion-cluster collisions. We know, for instance, that single-electron capture dominates ion-atom collisions at low impact velocities (i.e., when the projectile velocity is smaller than that of target electrons), but can one use ion-atom intuitions to analyze ion-cluster collisions? Is electron capture an efficient way to create positively charged clusters? Are there other processes competing efficiently with electron capture? Which are the relevant impact energy ranges?

The aim of the present work is to find answers to these questions and to provide quantitative cross sections for electron capture and excitation in the low impact energy range.

For this purpose, we have chosen the simplest ion,  $\text{H}^+$ , and a medium-size closed-shell metal cluster,  $\text{Na}_{20}$ . Since there are 20 *active* electrons in  $\text{Na}_{20}$ , one must use a truly many-electron time-dependent theory. The easiest way to achieve this goal is to work in the framework of the independent-electron model (IEM). A sample of results obtained within this model will be presented elsewhere [14]. In the present paper we develop the theory in detail and present a systematic study of electron capture and excitation in  $\text{H}^+ + \text{Na}_{20}$  collisions for impact energies between 40 and 500 eV.

When using the IEM, the first problem is to build realistic one-electron potentials that take into account the effect of all the electrons. In most previous works (see, e.g., [15]), this kind of collision has been investigated using simple phenomenological cluster potentials. However, isolated  $\text{Na}_{20}$  clusters can be accurately described using density functional (DF) or Hartree-Fock (HF) theories [2,16]. Hence it seems desirable that dynamical studies make use of the latter high-quality potentials. Since closed-shell metal clusters are practically spherical, the problem has the same global symmetry as in ion-atom collisions. Consequently, the language and techniques to be used in the study of  $\text{H}^+ - \text{Na}_{20}$  collisions will be close to the ones used in ion-atom collisions. The second problem is to evaluate cross sections that are directly measurable in experiments. As the number of active electrons  $N$  is very large, many different processes are possible. However, experiments do not provide information on a single final  $N$  configuration but on a series of states in which some levels are occupied irrespective of the occupation of the rest. For instance, it seems possible to design experiments to detect the number of captured electrons and the final state of the projectile, but it seems very unlikely that the experiments provide detailed information about electrons remaining in the cluster. Consequently, all those processes leading to the same final state of the projectile will contribute to the mea-

sured cross section. This corresponds to what has been called in the literature an *inclusive* cross section [17,18].

The paper is organized as follows. In Sec. II B we explain the theory we have used to obtain the cluster potentials, namely, our implementation of the spherical jellium model using a local-density approximation with exchange, correlation, and a self-interaction correction (LDAXC-SIC) [16]—the latter correction ensures the correct asymptotic behavior  $-1/r$  of the potential, which is crucial in the present case because the capture process occurs mainly at large distances. The basic ingredients of the formalism of *inclusive* probabilities are presented in Sec. II C. In Sec. II D we briefly summarize the *molecular* method, which has been widely used in ion-atom collisions and we have adopted here to solve the time-dependent Schrödinger equation. Our results are presented and discussed in Sec. III. We end the paper with some conclusions in Sec. IV. Atomic units are used throughout unless otherwise stated.

## II. THEORETICAL METHOD

### A. General considerations

In this work we consider collision velocities in the range  $v_{\text{col}} \sim 0.04 - 0.14$  a.u. These velocities are much smaller than the orbital velocities of the cluster electrons near the Fermi level,  $v_F \sim 0.6$  [16]. Hence, according to the theoretical models used in ion-atom collisions, the present situation corresponds to the low energy regime. It justifies the use of a molecular picture to analyze the collision dynamics.

We will see below that electron transfer takes place at large impact parameter ( $b_{\text{max}} \sim 20 - 30$  a.u.). At the impact energies considered here, this corresponds to a collision time  $\tau_{\text{col}} \sim 2b_{\text{max}}/v_{\text{col}} \sim (0.7 - 3.6) \times 10^{-14}$  s. The characteristic time  $\tau_v$  associated with the interaction between sodium atoms inside the cluster (period of vibration) is  $\tau_v \sim 10^{-12}$  s [19]. This time is very long compared to  $\tau_{\text{col}}$  and, consequently, the ionic background of the cluster will remain frozen during the collision.

Besides electron capture, the proton may lead to electronic excitations of the cluster. This excess energy relaxes with a lifetime  $\tau_{\text{rel}} \sim 10^{-13} - 10^{-12}$  s among the numerous internal modes through electron-phonon coupling [20]. When the energy deposit is larger than the lowest dissociation energy, the cluster may dissociate later on. However,  $\tau_{\text{rel}}$  being much larger than  $\tau_{\text{col}}$ , dissociation processes resulting from energy relaxation can be ignored during the collision. Still, dissociation might be induced in frontal collisions with the projectile, but this possibility will not be taken into account in our model. This is not a serious drawback of the theory provided that the capture mechanism takes place at long distances, as is the case for proton- $\text{Na}_{20}$  collisions.

Finally, some comments are appropriate concerning possible plasmon excitation during the collision. The plasmon energy for  $\text{Na}_{20}$  is about 3 eV [16]. At the low collision energy considered in this work, the frequency associated to  $\tau_{\text{col}}$  being much smaller than the plasmon frequency, there will be no plasmon excitation during the collision process.

### B. Cluster description

The cluster is described in the spherical background jellium model. This model consists in replacing the real ionic

core potential by a constant positive background corresponding to a uniformly distributed charge density. For a metal cluster having  $A$  singly charged ionic cores, this potential is given by

$$V_{\text{jel}}(r) = \begin{cases} -\frac{A}{2R_C} \left[ 3 - \left( \frac{r}{R_C} \right)^2 \right] & \text{for } r \leq R_C \\ -\frac{A}{r} & \text{for } r > R_C, \end{cases} \quad (1)$$

where  $R_C = A^{1/3} r_s$  and  $r_s$  is the Wigner-Seitz radius. For  $\text{Na}_{20}$ ,  $R_C = 10.5$  a.u. In the Kohn-Sham formulation of density functional theory, the ground-state electronic density  $\rho_C$  of an  $N$ -electron system is written in terms of single-particle orbitals  $\phi_i$ :

$$\rho_C(\mathbf{r}) = \sum_{i=1}^N \rho_i(\mathbf{r}) = \sum_i |\phi_i(\mathbf{r})|^2. \quad (2)$$

These orbitals obey the Schrödinger equation

$$\left[ -\frac{1}{2} \nabla^2 + V_{\text{KS}}(\mathbf{r}) \right] \phi_i(\mathbf{r}) = \epsilon_i \phi_i(\mathbf{r}), \quad (3)$$

where  $V_{\text{KS}}(\mathbf{r})$  is an effective single-particle potential given by

$$V_{\text{KS}}(\mathbf{r}) = V_{\text{jel}}(\mathbf{r}) + V_H(\rho_C(\mathbf{r})) + V_{\text{xc}}(\rho_C(\mathbf{r})), \quad (4)$$

where  $V_H(\rho_C(\mathbf{r}))$  is the Hartree potential and  $V_{\text{xc}}(\rho_C(\mathbf{r}))$  the exchange-correlation potential. Since the form of  $V_{\text{xc}}$  is not known in general, several approximations have been proposed in the literature. In this work, we have used the one obtained by Gunnarsson and Lundqvist [21] in the framework of the local-density approximation (LDA):

$$V_{\text{xc}}(\rho_C(\mathbf{r})) = -\left( \frac{3\rho_C(\mathbf{r})}{\pi} \right)^{1/3} - 0.0333 \ln \left( 1 + \frac{11.4}{r_s(\mathbf{r})} \right), \quad (5)$$

where  $r_s(\mathbf{r}) = [3/4\pi\rho_C(\mathbf{r})]^{1/3}$  is the local Wigner-Seitz radius. For a neutral cluster, the asymptotic behavior of  $V_{\text{KS}}$  is given by the exchange contribution to  $V_{\text{xc}}$ , which behaves at large distance as  $\rho_C(\mathbf{r})^{1/3}$ . As a consequence, the Kohn-Sham potential  $V_{\text{KS}}$  decreases exponentially to zero, i.e., it does not reproduce the correct  $1/r$  asymptotic behavior. This problem does not appear in Hartree-Fock theory, because the HF exchange potential exactly compensates the self-interaction term contained in the Hartree potential. Following Perdew and Zunger [22], we have added a self-interaction correction (SIC) that restores the correct asymptotic behavior of the potential (we will call this method LDAXC-SIC). This procedure has been successfully applied to the study of both ground- and excited-state properties of small metal clusters [16,23–25]. The corrected Kohn-Sham potential  $V_{\text{SIC}}^i$  is then given by

$$V_{\text{SIC}}^i(\mathbf{r}) = V_{\text{jel}}(\mathbf{r}) + \int \frac{[\rho_C(\mathbf{r}') - \rho_i(\mathbf{r}')] d\mathbf{r}'}{|\mathbf{r} - \mathbf{r}'|} + V_{\text{xc}}[\rho_C(\mathbf{r})] - V_{\text{xc}}[\rho_i(\mathbf{r})], \quad (6)$$

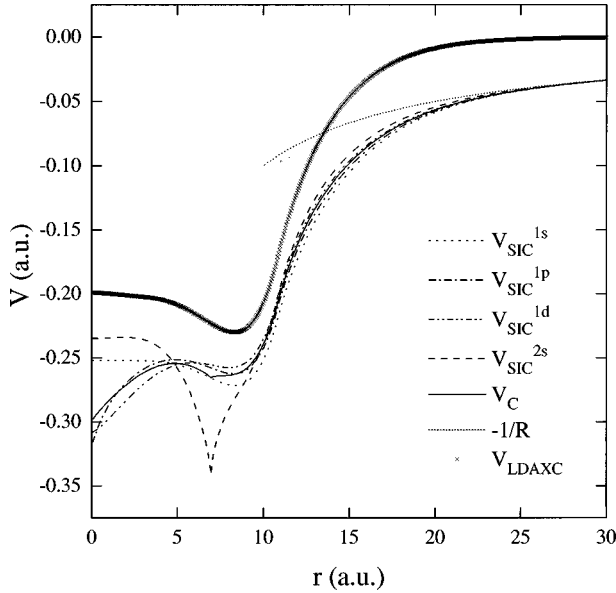


FIG. 1. Comparison between the  $V_{\text{SIC}}^i$  potentials, the LDAXC one, and the average potential  $V_C$  (see text). The figure also shows the function  $-1/R$ .

where  $\rho_i$  is the  $i$  single-particle density defined in Eq. (2). It is easy to check that, as in HF theory, the resulting potential has the correct  $1/r$  behavior at large distances. Notice also that the  $V_{\text{SIC}}^i$  potential is now explicitly state dependent. Figure 1 shows a comparison between the original LDAXC potential and the calculated  $V_{\text{SIC}}^i$  potentials for the occupied orbitals  $1s$ ,  $1p$ ,  $1d$ , and  $2s$  of  $\text{Na}_{20}$ . The corresponding energy eigenvalues are given in Table I.

Similarly to Koopman's theorem in HF theory, the energy of the highest occupied (HO) orbital resulting from *exact* Kohn-Sham calculations is an excellent approximation to the cluster ionization potential. In fact, it is also a good approximation for the *approximate* LDAXC-SIC theory, as illustrated by the good agreement between the  $2s$  energy reported in Table I (3.84 eV) and the experimental ionization potential (3.77 eV) [26]. This means that the eigenvalue and eigenfunction associated to the HO orbital can be interpreted as the particle energy and wave function, respectively. Although this cannot be proved for other Kohn-Sham eigenvalues and eigenfunctions (see Ref. [2] for a detailed discussion), one can expect, however, this interpretation to provide reasonable approximations to the actual single-particle properties. This is supported by the fact that most of the collision dynamics occurs far from the cluster surface, where the  $V_{\text{SIC}}^i$

TABLE I. Eigenenergies (atomic units) of the occupied single-particle states of  $\text{Na}_{20}$  calculated in the local-density approximation with exchange, correlation, and self-interaction correction. The energies  $\langle \epsilon_j \rangle$  are those obtained by using the average potential of Eq. (7).

Orbital	$\epsilon_j$	$\langle \epsilon_j \rangle$
$1s$	-0.233	-0.230
$1p$	-0.199	-0.200
$1d$	-0.159	-0.163
$2s$	-0.141	-0.150

potentials do not differ appreciably from the HF ones. This is clearly shown in Fig. 1 for  $r > 9$  a.u. In fact, the state-dependent  $V_{\text{SIC}}^i$  potentials can be replaced in this region by a common average potential

$$V_C(r) \equiv \langle V_{\text{SIC}}(r) \rangle = \frac{1}{N} \sum_k V_{\text{SIC}}^k(r) n_k, \quad (7)$$

where the summation is performed over all occupied orbitals and  $n_k$  denotes the number of electrons in subshell  $k$ . It can be seen in Table I that the single-particle energies resulting from this average potential are practically identical to those obtained with the state-dependent potentials  $V_{\text{SIC}}^i$ . As we will see in the next section, the scattering problem is greatly simplified by using the same effective potential for all active electrons, since the single-particle orbitals are orthogonal and the total Hamiltonian can be written as a sum over identical single-particle Hamiltonians.

The  $V_C$  potential of the isolated cluster has been obtained numerically using Eqs. (3), (6), and (7). For practical reasons, we have fitted  $V_C$  to an analytical function. More specifically, we have rewritten the potential in the following way:

$$V_C(r) = \lim_{\epsilon \rightarrow 0} \left\{ V_C(r) \Theta_\epsilon(r) - \frac{1}{r} [1 - \Theta_\epsilon(r)] \right\}, \quad (8)$$

where  $\Theta_\epsilon$  is a ‘‘step’’ function fulfilling

$$\Theta_\epsilon(r) \approx \begin{cases} 1, & r < r_0 - \epsilon \\ 0, & r > r_0 + \epsilon. \end{cases} \quad (9)$$

For  $\text{Na}_{20}$ , we have chosen  $r_0 = 25$  a.u. Then, for a small enough  $\epsilon$ , we have least-squares fitted the two functions  $\Theta_\epsilon V_C$  and  $\Theta_\epsilon$ , using a linear combination of 30 Gaussian functions placed on the cluster center. The resulting analytical potential is identical to the one shown in Fig. 1 to a precision of  $10^{-6}$ . The advantage of such a procedure is that all matrix elements involving  $V_C$  and the Gaussian-type orbitals (GTO) used to describe the compound system  $(\text{Na}_{20}\text{-H})^+$  (see Sec. II D) can be performed analytically.

### C. Inclusive cross sections

As explained above, all cluster electrons are affected by, to a good degree of approximation, the same average potential. Thus, for an isolated cluster, it is reasonable to use the independent-electron model. Here, we assume that the IEM is still valid in the presence of the proton potential. Of course, this is not completely true: the proton induces a polarization potential that affects each electron differently. Indeed, as is well known, the projectile polarizes the cluster which in turn exerts an attractive force on the projectile. The equivalent classical picture is given in electrostatics by the presence of an image charge [27]. Therefore the potential affecting a given electron will be affected by the polarization of the whole electronic cloud. However, since the leading term of the polarization potential decreases as  $1/R^4$ , its relative importance decreases rapidly with  $R$ . Consequently, in all dynamical calculations reported in this work we will use the average potential  $V_C$  discussed in the preceding section.

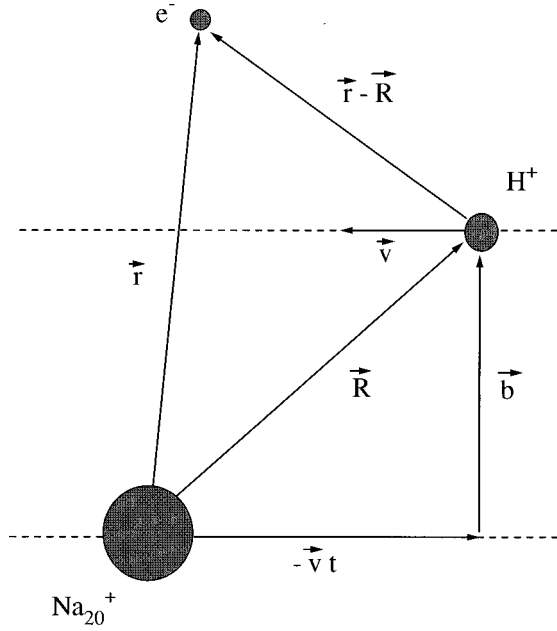


FIG. 2. Geometry of the  $(\text{H-Na}_{20})^+$  system.

In the independent-electron approximation, the total  $N$ -electron Hamiltonian  $\hat{\mathcal{H}}$  is written as a sum of one-electron effective Hamiltonians,  $\hat{h}(i)$ ,

$$\hat{\mathcal{H}} = \sum_{i=1}^N \hat{h}(i). \quad (10)$$

The  $\hat{h}$  Hamiltonian is given by

$$\hat{h} = -\frac{1}{2}\nabla^2 + V_p(|\mathbf{r}-\mathbf{R}|) + V_C(\mathbf{r}), \quad (11)$$

where  $V_p$  is the proton Coulomb potential,  $V_p = -1/|\mathbf{r}-\mathbf{R}|$ , and  $V_C$  is the average potential defined in Eq. (7). Notice that the origin of electronic coordinates has been placed on the cluster center. The geometry of such a system is displayed in Fig. 2.

Now, we treat the collision in the framework of the impact parameter method (IPM), i.e., the projectile follows a straight line trajectory whereas the electrons are described quantum mechanically. In the IEM approximation, two equivalent methods can be used to solve the  $N$ -particle problem using a basis of  $n$  one-electron spin orbitals ( $n > N$ ). In a ‘‘full’’ many-particle approach, one usually expands the time-dependent wave function in terms of  $\approx \binom{n}{N}$  Slater determinants. The transition amplitudes are then the solution of  $\approx \binom{n}{N}$  coupled differential equations. An alternative method is to consider the evolution of each electron independently by solving  $N$  one-electron problems which lead to  $N$  sets of  $n$  one-electron amplitudes.  $N$ -electron amplitudes obtained in both ways are related exactly, but the second method is computationally less involved [28].

Let us assume that each electron  $i$  is initially in a  $\phi_i(\mathbf{r})$  spin orbital of energy  $\epsilon_i$ . Then, we have to solve a set of  $N$  time-dependent Schrödinger equations

$$\hat{h}\psi_i(\mathbf{r},t) = i\frac{d}{dt}\psi_i(\mathbf{r},t), \quad i=1,\dots,N \quad (12)$$

where each  $\psi_i(\mathbf{r},t)$  wave function is subject to the initial condition

$$\lim_{t \rightarrow -\infty} \psi_i(\mathbf{r},t) = \phi_i(\mathbf{r}) \exp[-i\epsilon_i t] \quad (13)$$

and fulfills the orthogonality condition

$$\langle \psi_i(\mathbf{r},t) | \psi_j(\mathbf{r},t) \rangle = \delta_{ij} \quad (14)$$

for all  $t$ . The transition probability from a specific initial configuration given by the Slater determinant  $(i_1, \dots, i_N) = \|\phi_{i_1} \cdots \phi_{i_N}\|$  to a specific final configuration  $(f_1, \dots, f_N) = \|\phi_{f_1} \cdots \phi_{f_N}\|$  is given by

$$P_{f_1, \dots, f_N} = |\langle \psi_{i_1} \cdots \psi_{i_N}, t = +\infty | f_1 \cdots f_N \rangle|^2, \quad (15)$$

which is called *exclusive probability* [29] and can be written as a  $(N \times N)$  determinant

$$P_{f_1, \dots, f_N} = \det(\gamma_{nn'}), \quad n, n' = 1, \dots, N \quad (16)$$

where  $\gamma_{nn'}$  is the one-particle density matrix

$$\gamma_{nn'} = \langle f_n | \hat{\rho} | f_{n'} \rangle \quad (17)$$

and  $\hat{\rho}$  is the density operator which accounts for the time evolution of the spin orbitals:

$$\hat{\rho}(\mathbf{r}, \mathbf{r}') = \sum_{i=1}^N |\psi_i(\mathbf{r}, t = \infty)\rangle \langle \psi_i(\mathbf{r}', t = \infty)|. \quad (18)$$

As discussed in the Introduction, the experiments do not detect all the electrons at the end of the collision but only some of them and possibly some vacancies. For this reason, it is more useful to evaluate *inclusive probabilities* that can be directly compared with experiment. The inclusive probability  $P_{f_1, \dots, f_q}$  of finding  $q$  of the  $N$  electrons in the sub-configuration  $(f_1, \dots, f_q)$  while the remaining  $N-q$  electrons occupy any other states is given by an ordered sum over all exclusive probabilities which include that sub-configuration:

$$P_{f_1, \dots, f_q} = \sum_{f_{q+1} < \dots < f_N} P_{f_1, \dots, f_N}, \quad q < N \quad (19)$$

which from Eq. (16) is a sum of  $(N \times N)$  determinants. However, using the closure relation and orthogonality of the  $\psi_i$  spin orbitals [see Eq. (14)], it can be shown [18] that the inclusive probability is given by the  $(q \times q)$  determinant:

$$P_{f_1, \dots, f_q} = \det(\gamma_{nn'}), \quad n, n' = 1, \dots, q, \quad q < N. \quad (20)$$

The inclusive probability for a configuration with  $q$  occupancies and  $L-q$  holes, in terms of inclusive probabilities related only to occupancies, is given by [18]

$$\begin{aligned}
P_{f_1, \dots, f_q}^{f_{q+1}, \dots, f_L} &= P_{f_1, \dots, f_q} - \sum_{f_{q+1}} P_{f_1, \dots, f_q, f_{q+1}} \\
&+ \sum_{f_{q+1} < f_{q+2}} P_{f_1, \dots, f_q, f_{q+1}, f_{q+2}} \dots \\
&+ (-1)^{L-q} P_{f_1, \dots, f_q, f_{q+1}, \dots, f_L}, \quad (21)
\end{aligned}$$

where occupancies are indicated by subscripts and vacancies by superscripts. The inclusive probabilities (20) and (21) are associated to a sum of processes and take into account the Pauli exclusion principle. The one-particle density operator (18) includes spin orbitals with both spin up ( $\alpha$ ) and down ( $\beta$ ). It can be formally written

$$\hat{\rho} = \hat{\rho}^\alpha + \hat{\rho}^\beta, \quad (22)$$

where the first operator is responsible for scattering of  $\alpha$  electrons and the second one for  $\beta$  electrons. In our description, spin will be preserved during the collision because we neglect spin-orbit coupling. Therefore  $\alpha$  spin orbitals will not be coupled to  $\beta$  spin orbitals and, from Eq. (22), we can write

$$P_{f_1, \dots, f_{l_\alpha}, f_{l_\alpha+1}, \dots, f_l} = P_{f_1, \dots, f_{l_\alpha}}^\alpha P_{f_{l_\alpha+1}, \dots, f_l}^\beta, \quad (23)$$

where  $l_\alpha$  is the number of electrons with spin  $\alpha$ , and  $P^\alpha$  and  $P^\beta$  are inclusive probabilities involving  $\rho^\alpha$  and  $\rho^\beta$ , respectively. Then, the inclusive probability  $P_{f_1, \dots, f_q}^{f_{q+1}, \dots, f_L}$  defined in Eq. (21) can be obtained from  $P^\alpha$  and  $P^\beta$  probabilities. Spin orbitals which are described by the same spatial part during the collision lead to one-electron transition amplitudes which are identical. Therefore only one transition probability must be evaluated for each doubly occupied orbital.

#### D. The “molecular” method

The set of time-dependent Schrödinger equations (12) has been solved by expanding the one-electron wave functions  $\psi_i(\mathbf{r}, t)$  in a basis of Born-Oppenheimer (BO) *molecular* states  $\{\chi_k(\mathbf{r}, R)\}$ :

$$\psi_i(\mathbf{r}, t) = \sum_k c_{ik}(t) \chi_k(\mathbf{r}, R) \exp\left[-i \int_0^t E_k(R) dt'\right], \quad (24)$$

where the  $E_k$  energies are the BO adiabatic energies associated to the  $\{\chi_k(\mathbf{r}, R)\}$  states:

$$\hat{h} \chi_k(\mathbf{r}, R) = E_k(R) \chi_k(\mathbf{r}, R). \quad (25)$$

Equation (25) has been solved by expanding the BO states in a two-center *atomic* basis built from spherical GTOs as described in the Appendix. Notice that expansion (24) does not include translation factors. Since the origin of electronic coordinates has been placed on the heaviest center (i.e., on the  $\text{Na}_{20}$  cluster) and the collision velocities considered in this work are rather small, we do not expect translation factors to be important for the present collisional study. Substitution of Eq. (24) in the time-dependent Schrödinger equation (12) leads to the system of coupled differential equations:

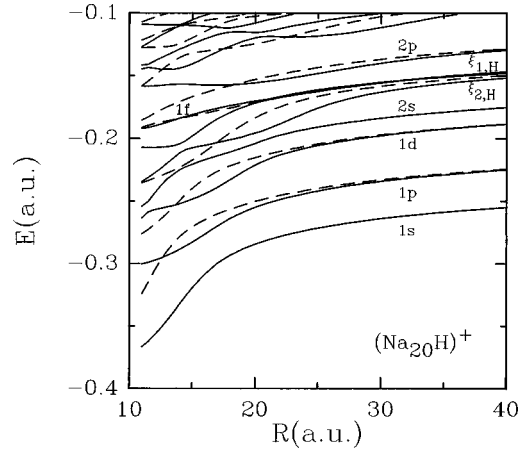


FIG. 3. Adiabatic potential energy curves of  $(\text{H-Na}_{20})^+$ . Full lines:  $\sigma$  states; dashed lines:  $\pi$  states. Curves for other symmetries are not shown because they correspond to states that are irrelevant for the collisional study.

$$i \frac{dc_{ik}}{dt} = \sum_{l \neq k} \left\langle \chi_k \left| -i \frac{d}{dt} \right| \chi_l \right\rangle c_{il} \exp\left[-i \int_0^t (E_l - E_k) dt'\right], \quad (26)$$

where the coupling matrix elements  $\langle \chi_k | -i d/dt | \chi_l \rangle$  have the usual radial and rotational components in the molecule reference frame [30]. The use of the GTO basis ensures that all the couplings can be evaluated analytically. The systems of equations (26) have been solved using the program SUPERPAMPA [31].

### III. RESULTS AND DISCUSSION

#### A. Adiabatic energies and couplings

We show in Fig. 3 the adiabatic potential energy curves for the  $\sigma$  and  $\pi$  states of the  $(\text{Na}_{20}\text{-H})^+$  molecule [see Eq. (25)], and in Fig. 4 a set of radial couplings that are relevant

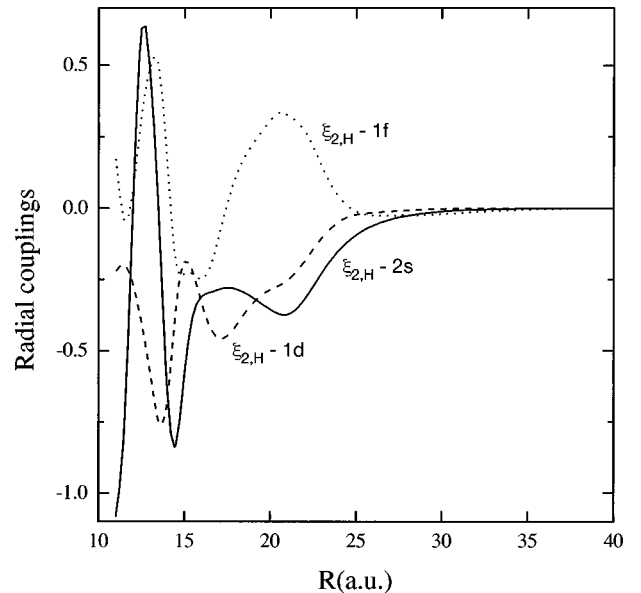


FIG. 4. Radial couplings between the  $\xi_{2,H}$  state and the  $2s$ ,  $1d$ , and  $1f$  states of  $\sigma$  symmetry.

for the understanding of the dynamics. For simplicity, the molecular orbitals are labeled using the separate ‘‘atom’’ (SA) notation (i.e., that corresponding to infinitely separated  $H^+$  and  $Na_{20}$  or  $H$  and  $Na_{20}^+$ ). In the SA limit, hydrogen orbitals include a subscript H, whereas cluster orbitals do not. It must be also noticed that the excited H orbitals ( $n = 2, 3, \dots$ ) are in fact Stark hybrids due to the cluster electric field. For the  $\sigma(n=2)$  orbitals of H, we will use the notation  $\xi_{1,H} = (2s_H + 2p_{0,H})/\sqrt{2}$  and  $\xi_{2,H} = (2s_H - 2p_{0,H})/\sqrt{2}$ .

Figure 3 shows that the  $\sigma$  molecular orbitals denoted  $1s$ ,  $1p$ ,  $1d$ , and  $2s$  (i.e., those connected to the available entrance channels) strongly interact with the  $\sigma$  orbitals correlated with the  $n=2$  orbitals of hydrogen. The corresponding radial couplings present maxima at  $R \approx 20$  a.u., thus showing that capture to the  $H(n=2)$  orbitals must take place far beyond the cluster surface. The radial couplings between  $\pi$  states (not shown) are important at smaller  $R$  (see in Fig. 3, for instance, that the avoided crossing between the  $2p_{\pi,H}$  state and the  $1d_{\pi}$  one occurs at  $R \approx 15$  a.u.). Therefore one can expect the role of initially occupied  $\pi$  states to be less important than that of  $\sigma$  states, which is further supported by the fact that  $\sigma$ - $\pi$  rotational couplings contributing to the capture process are not important around  $R \approx 20$  a.u.

It must be pointed out that the energy spacing between cluster states is much smaller than that of hydrogen states. This is crucial to understand the dynamics of the collision. For instance, at low collision energies, this implies that the capture reaction must lead to the formation of  $H(n=2)$  almost exclusively. Indeed, the energy scale used in Fig. 3 shows that the  $H(1s)$  state lies far below in energy, so that it cannot be efficiently populated. Similar arguments apply to more excited states of H, and to cluster orbitals above the empty  $2p$  one.

In view of the previous discussions, in this work we will limit the expansion in Eq. (24) to the following molecular states of  $\sigma$  symmetry: the two states dissociating into the  $\xi_{1,H}$  and  $\xi_{2,H}$  states of H, the four states dissociating into occupied orbitals of the cluster, namely  $1s$ ,  $1p$ ,  $1d$ , and  $2s$ , and the states dissociating into the empty  $1f$  and  $2p$  orbitals of the cluster. This amounts to eight states. This minimal set of molecular states will allow us to describe the capture reaction as well as cluster excitation.

### B. Transition probabilities and cross sections

First we have evaluated the inclusive probabilities  $P_{\xi_{1,H}}$  and  $P_{\xi_{2,H}}$ , which represent the probability of capture to the  $\xi_{1,H}$  and  $\xi_{2,H}$  states of H, irrespective of the processes experienced by the other electrons. These probabilities include electron capture and capture excitation. Thus the calculated probabilities do not correspond to an *exclusive* single-capture reaction, but to a sum of reactions whose common feature is to yield hydrogen atoms with at least one electron. As capture of more than one electron is very unlikely (it would lead at most to the formation of  $H^-$ , which is a weakly bound negative ion),  $P_{\xi_{1,H}}$  and  $P_{\xi_{2,H}}$  can be interpreted as the probabilities of finding *one* electron in the projectile. In other words, we are assuming that double-capture and higher-order capture cross sections are exactly zero. Nevertheless, all the

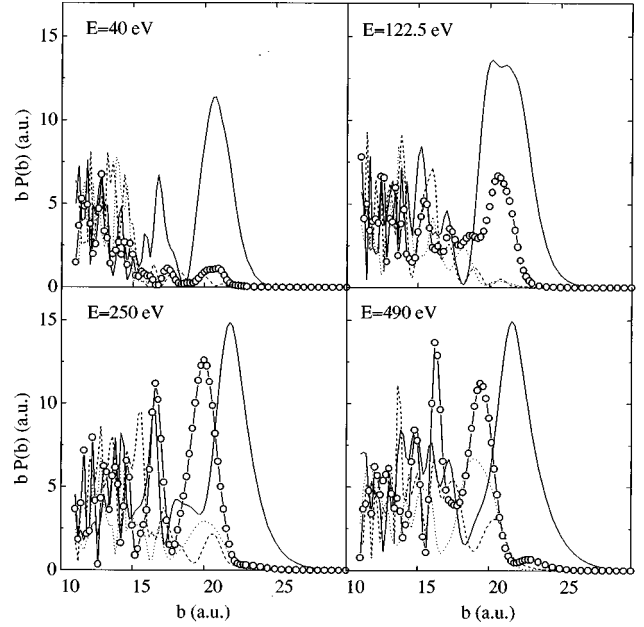


FIG. 5. Transition probabilities  $P_j$  times  $b$  as functions of  $b$ . Full line:  $P_{\xi_{2,H}}$ ; dashed line:  $P_{\xi_{1,H}}$ ; line with open circles:  $P_{1f}$ ; dotted line:  $P_{2p}$ .

other multiple processes such as capture excitation and multiple excitation are properly described in our model and, hence, they are included in the calculated inclusive probabilities.

In Fig. 5 we have plotted  $bP_{\xi_{1,H}}$  and  $bP_{\xi_{2,H}}$  as functions of  $b$  at several impact energies. It can be seen that the largest contribution to the total capture cross section comes from the region around  $b \sim 20-30$  a.u., which is far apart from the cluster surface. In the same figure we have included  $bP_{1f}$  and  $bP_{2p}$ , which are the probabilities of finding an excited electron in the  $1f$  and  $2p$  orbitals, respectively. These probabilities are smaller than  $bP_{\xi_{2,H}}$ , but the largest contributions to the excitation process come again from a region far from the cluster surface ( $b \approx 20$  a.u.). These results support our assumption that capture and excitation reactions can be studied by neglecting fragmentation effects occurring at short impact parameters (frontal impact).

We define now the total capture probability  $\hat{P}_{n=2,H} = 2(P_{\xi_{1,H}} + P_{\xi_{2,H}})$ . Although addition of two inclusive probabilities may lead to overcounting in some cases [28], this problem does not exist here because the only configurations included in both  $P_{\xi_{1,H}}$  and  $P_{\xi_{2,H}}$  are those with two or more electrons on the projectile, which, as discussed above, barely contribute to the total probability. The factor of 2 appears because the captured electron can have either  $\alpha$  or  $\beta$  spin components. Similarly, we define the *excitation* probabilities as  $\hat{P}_i = 2P_i - (P_i)^2$ , where  $i$  stands for either  $1f$  or  $2p$ . The  $(P_i)^2$  term, which corrects for overcounting, cannot be neglected in the present case. The corresponding cross sections have been evaluated using the formula

$$\sigma_i = 2\pi \int_{b_0}^{\infty} b \hat{P}_i db, \quad (27)$$

where  $b_0 = R_C$ . By using this lower limit for the integral, we

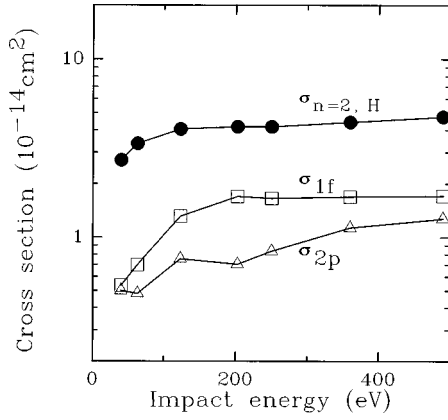


FIG. 6. Capture and excitation cross sections for  $H^+ + Na_{20}$  collisions.

assume that trajectories penetrating the cluster give negligible contributions to the cross sections. The calculated cross sections are shown in Fig. 6. The values of these cross sections are much larger than those observed, for instance, in  $H^+ - Na$  collisions [32,33] ( $\sim 1.5 \times 10^{-15} \text{ cm}^2$  at 500 eV). It can also be seen that the capture cross section increases rapidly up to  $E \approx 200$  eV and then remains almost flat. This behavior is qualitatively similar to that observed in  $H^+ - Na$  collisions, but the flat region is reached much earlier in the present case. The  $\sigma_{1f}$  and  $\sigma_{2p}$  cross sections present similar behaviors. In particular,  $\sigma_{1f}$  is only two to three times smaller than  $\sigma_{n=2,H}$ . One must stress here that the  $\sigma_{1f}$  and  $\sigma_{2p}$  cross sections cannot be interpreted as pure excitation cross sections: these cross sections include contributions from capture excitation. The importance of the capture-excitation mechanism is illustrated in Fig. 7 by comparing  $P_{\xi_{2,H}}$  and  $P_{\xi_{2,H}}^{1f\bar{1}f2p\bar{2}p}$  (orbitals with and without bars correspond to  $\beta$  and  $\alpha$  spin components, respectively). As explained above, the first inclusive probability,  $P_{\xi_{2,H}}$ , includes

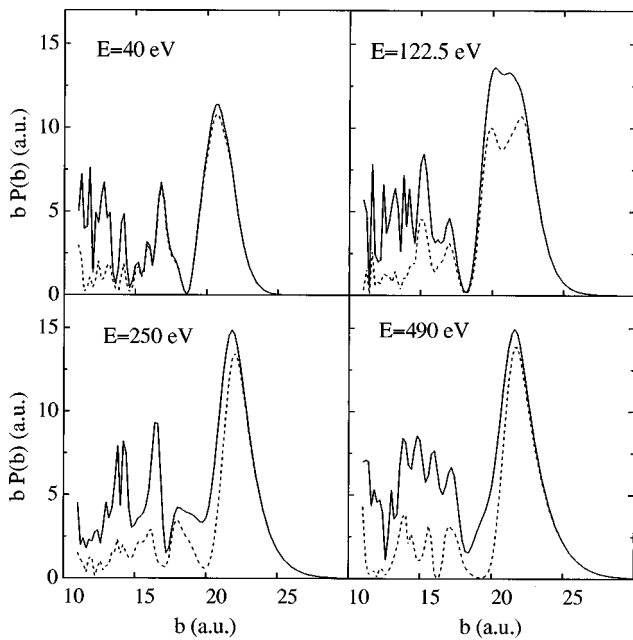


FIG. 7. Comparison between the transition probabilities  $P_{\xi_{2,H}}$  (full line) and  $P_{\xi_{2,H}}^{1f\bar{1}f2p\bar{2}p}$  (dashed line).

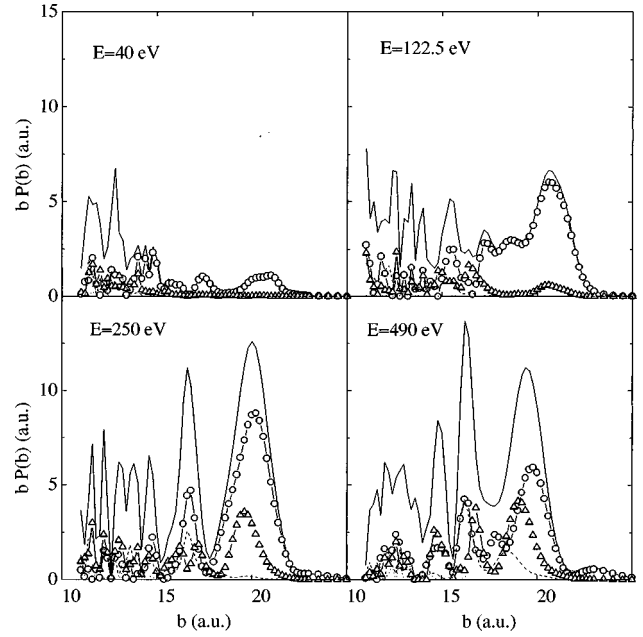


FIG. 8. Comparison between the transition probabilities  $P_{1f}$  (full line) and  $P_{\xi_{1,H}\xi_{2,H}}^k$  where  $k=1s$  (dotted line),  $k=1p$  (dashed line),  $k=1d$  (line with open triangles), and  $k=2s$  (line with open circles).

all processes leading to capture in the  $\xi_{2,H}$  orbitals, in particular, all possible capture-excitation channels that can be described with our minimal basis. In contrast, capture-excitation channels are excluded in  $P_{\xi_{2,H}}^{1f\bar{1}f2p\bar{2}p}$ , because the  $1f$  and  $2p$  orbitals remain empty. Then the difference between these probabilities will be due to the capture-excitation mechanism. It can be seen in Fig. 7 that capture-excitation processes exist even at the lowest energy reported in this work and that its relative importance increases with impact energy. Thus, at variance with ion-atom collisions, many-electron processes are important even at low impact energies.

Another point of interest is to investigate the origin of the vacancies produced by both capture and excitation mechanisms. This information can be very useful in estimating the energy deposited in the cluster as a result of the collision. Knowledge of the energy deposit is essential to determine if neutral and singly charged clusters remain stable after the collision or, on the contrary, they undergo fragmentation. In order to extract this information, we have evaluated the following inclusive probabilities:  $P_{1f}^{\xi_{1,H}\xi_{2,H}}$ ,  $P_{1f}^{\xi_{1,H}\xi_{2,H}^{1s}}$ ,  $P_{1f}^{\xi_{1,H}\xi_{2,H}^{1p}}$ ,  $P_{1f}^{\xi_{1,H}\xi_{2,H}^{1d}}$ , and  $P_{1f}^{\xi_{1,H}\xi_{2,H}^{2s}}$ . The first one,  $P_{1f}^{\xi_{1,H}\xi_{2,H}}$ , represents *pure*  $1f$  excitation because projectile orbitals remain empty; the  $P_{1f}^{\xi_{1,H}\xi_{2,H}^k}$  probabilities represent *pure* excitation from a given initially occupied orbital  $k$ . Figure 8 shows that, at low energies, excited electrons come preferentially from the  $2s$  orbital. At higher energies, contributions from the  $1d$  and  $1p$  orbitals become increasingly important and, at 500 eV, formation of  $2s$  and  $1d$  holes is equally probable. We can obtain similar information for the captured electrons by comparing  $P_{\xi_{2,H}}^{1f\bar{1}f2p\bar{2}p}$  with  $P_{\xi_{2,H}}^{1f\bar{1}f2p\bar{2}p^{1s}}$ ,  $P_{\xi_{2,H}}^{1f\bar{1}f2p\bar{2}p^{1p}}$ ,  $P_{\xi_{2,H}}^{1f\bar{1}f2p\bar{2}p^{1d}}$ , and  $P_{\xi_{2,H}}^{1f\bar{1}f2p\bar{2}p^{2s}}$ .

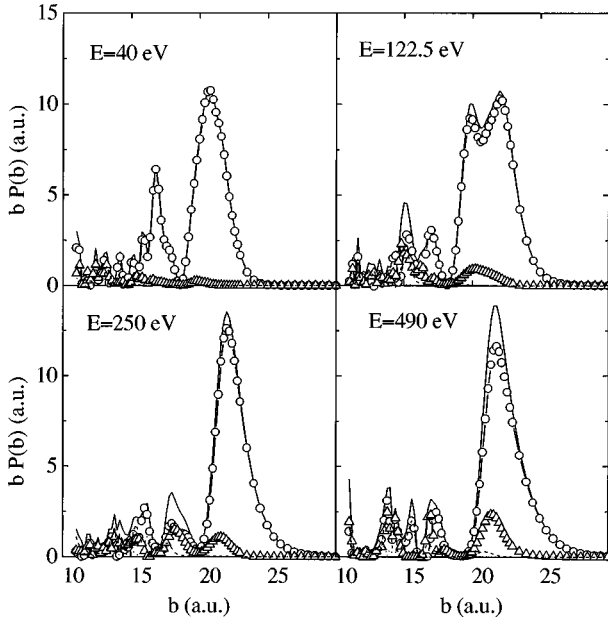


FIG. 9. Comparison between the transition probabilities  $P_{\xi_{2,H}}^{1f1f2p2p}$  (full line) and  $P_{\xi_{2,H}}^{1f1f2p2p,k}$  where  $k=1s$  (dotted line),  $k=1p$  (dashed line),  $k=1d$  (line with open triangles), and  $k=2s$  (line with open circles).

Figure 9 shows that captured electrons arise mainly from the  $2s$  orbital, even at high impact energies. Indeed, at 500 eV, there are practically no  $1s$  and  $1p$  holes, and formation of  $1d$  holes is still much less probable than formation of  $2s$  holes.

### C. Energy deposit

As mentioned above, when the collision is over, excited clusters can relax their energy excess among the various internal modes through electron-phonon coupling. If the energy excess is larger than the lowest dissociation energy, it may induce fragmentation of the cluster. In order to analyze this possibility, we have evaluated the energy deposit at a given impact energy using the approximate formula:

$$E^* = \frac{\sum_j (\sigma_{1f,j} \Delta E_{1f,j} + \sigma_{2p,j} \Delta E_{2p,j})}{\sum_j (\sigma_{1f,j} + \sigma_{2p,j})}, \quad (28)$$

where

$$\sigma_{f,j} = 2\pi \int_{b_0}^{\infty} 2b P_f^{\xi_{1,H}\xi_{2,H},j}(b) db, \quad (29)$$

$\Delta E_{f,j} = \epsilon_j - \epsilon_f$ ,  $f=1f$  or  $2p$ , and  $j$  stands for  $1s$ ,  $1p$ ,  $1d$ , and  $2s$ . Figure 10 shows the calculated energy deposit as a function of impact velocity. The energy deposit ranges from 1.1 eV to 1.4 eV, with a minimum around  $v_{col} = 0.07$  a.u. At higher energies,  $E^*$  is roughly proportional to the collision velocity, in agreement with the Lindhard model for collision velocities smaller than the Fermi velocity [34].

The most efficient decay channel for a neutral cluster such as  $\text{Na}_{20}^*$  is evaporation of a neutral monomer [35]. This cor-

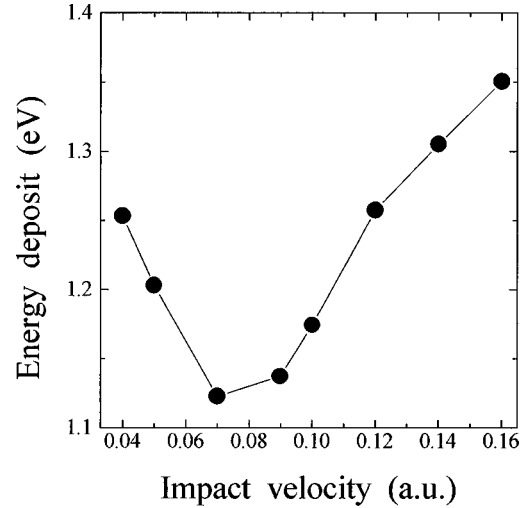


FIG. 10. Energy deposit as a function of impact velocity.

responds to the lowest dissociation channel, whose dissociation energy is 0.88 eV [35]. Consequently, excited  $\text{Na}_{20}^*$  clusters resulting from the collision of  $\text{Na}_{20}$  with protons will undergo dissociation into  $\text{Na}_{19} + \text{Na}$ . The corresponding evaporation time can be estimated using the statistical model of Weisskopf [36], which leads to  $\tau_{ev} \sim 10^5$  s. This means that the excited cluster will remain stable for a long time.

We have not evaluated the energy deposited in  $\text{Na}_{20}^+$  clusters because it is much smaller than the corresponding dissociation energy, which is 0.85 eV. Indeed, Fig. 9 shows that only a few  $\text{Na}_{20}^+$  clusters are produced in an excited state. Moreover, these excited clusters have a hole in the  $1d$  orbital, so that the energy deposit is approximately given by  $\epsilon_{2s} - \epsilon_{1d} \approx 0.4$  eV, which is not enough to induce dissociation. Consequently, positively charged clusters formed in the collision will remain stable.

## IV. CONCLUSION

In this paper we have studied the collision between protons and  $\text{Na}_{20}$  clusters in the impact energy range 40–500 eV. The cluster has been described in the framework of the Kohn-Sham formalism using a local-density approximation which includes exchange, correlation, and a self-interaction correction. The collision process has been treated semiclassically in the framework of the independent-electron model. We have evaluated cross sections for capture and excitation that can be directly compared with experiments and take into account the many-particle aspect of the problem. Our results show that electron capture is the dominant process in the whole energy range investigated here. The calculated cross section is of the order of  $(2-5) \times 10^{-14}$  cm<sup>2</sup> and it is much larger than the known cross sections for  $\text{H}^+$ -Na collisions. It includes the single-capture mechanism, but also capture excitation. The latter process is important even at low collision velocities. Cluster excitation is also a very important process since the corresponding cross sections are only two to three times smaller than capture cross sections. This behavior is in contrast with the one observed in ion-atom collisions. Excited neutral clusters may undergo fragmentation when the energy excess is larger than the lowest dissociation energy. For this reason we have investigated the origin of the vacan-

cies created during the collision and we have found that the energy deposit ranges from 1.1 to 1.4 eV. This suggests that  $\text{Na}_{20}^*$  mainly decays by ejecting one sodium atom and that the typical evaporation time is  $\sim 10^5$  s.

In summary, we have been able to characterize the dynamics of  $\text{H}^+$ - $\text{Na}_{20}$  collisions and to provide cross sections and energy deposits of experimental interest. The present methodology will be used in the future to investigate collisions involving more complicated clusters and other multiply charged ions.

#### ACKNOWLEDGMENTS

This work has been partially supported by the DGICYT Project No. PB93-0288-C02-01. F. M. acknowledges the Université de Metz for financial support. M. F. P. is grateful to the CNAM for traveling support. The authors would like to thank the CNUSC (Centre National Universitaire Sud de Calcul), the CIRIL (Centre Interuniversitaire de Recherche Informatique Lorrain), and the CCCFC (Centro de Computación Científica de la Facultad de Ciencias de la UAM) for their generous allocation of computer time.

#### APPENDIX

Both cluster and hydrogen orbitals have been represented in a basis of real spherical Gaussian-type orbitals:

$$\varphi_{kj}^{l|m|}(\mathbf{r}) = N_{kj} r^k \exp(-\alpha_j r^2) P_{l|m|}(\theta) \cos(|m|\phi), \quad (\text{A1})$$

where  $N_{kj}$  is a normalization constant and  $P_{l|m|}$  is an associated Legendre polynomial. For each GTO of a given  $m$ , we will use the notation  $(k, l, \alpha_j)$ . The cluster basis includes

TABLE II. Exponents  $\alpha_j$  of GTO basis set used to describe the atomic orbitals of hydrogen. See Eq. (A1) for notation.

$l=0$ $k=0$	$l=1$ $k=1$	$l=0$ $k=2$	$l=2$ $k=2$
0.0095	0.01	0.015	0.015
0.017	0.027	0.055	0.055
0.035	0.065	0.18	0.18
0.07	0.15		
0.15	0.30		
0.30	0.6		
0.6	1.2		
1.2	2.4		
2.4	4.8		
4.8	9.6		
9.6			
19.2			

GTOs with  $l=0, 1, 2$ , and  $3$ , and  $j=l$  and  $l+2$ . Namely, 15  $(0,0,\alpha_j)$ , 15  $(2,0,\alpha_j)$ , 15  $(1,1,\alpha_j)$ , 15  $(2,2,\alpha_j)$ , 8  $(3,1,\alpha_j)$ , and 8  $(3,3,\alpha_j)$  functions. The  $\alpha_j$  exponents are given by the formula  $\alpha_j = 0.00538 \times 1.7^{(j-1)}$ , where  $j=1,2,\dots,15$  for the former four groups and  $j=1,2,\dots,8$  for the last two groups. Hence the cluster basis amounts to  $76\sigma$ ,  $61\pi$ ,  $38\delta$ , and  $23\varphi$  orbitals. This basis reproduces the orbital energies of Table I up to six significant figures. The hydrogen basis is given in Table II and amounts to  $29\sigma$ ,  $14\pi$ , and  $3\delta$  orbitals, which lead to the exact  $n=1$  and  $n=2$  hydrogen energies up to six significant figures.

- [1] See, for instance, Z. Phys. D **40** (1997), and references therein.  
[2] M. Brack, Rev. Mod. Phys. **65**, 677 (1993).  
[3] W. A. de Heer, Rev. Mod. Phys. **65**, 611 (1993).  
[4] N. G. Gotts and A. J. Stace, Phys. Rev. Lett. **66**, 21 (1991).  
[5] A. Goerke, H. Palm, C. P. Schulz, F. Spiegelmann, and I. V. Hertel, J. Chem. Phys. **98**, 9635 (1993).  
[6] C. Bréchnignac, Ph. Cahuzac, J. Leygnier, R. Pflaum, and J. Weiner, Phys. Rev. Lett. **61**, 314 (1988).  
[7] C. Bréchnignac, Ph. Cahuzac, F. Carlier, J. Leygnier, and I. V. Herter, Z. Phys. D **17**, 61 (1990).  
[8] B. Walch, C. L. Cocke, R. Voelpel, and E. Salzborn, Phys. Rev. Lett. **72**, 1439 (1994).  
[9] M. Guissani and V. Sidis, J. Chem. Phys. **102**, 1288 (1995); Z. Phys. D **40**, 221 (1997).  
[10] H. Shen, P. Hvelplund, D. Mathur, A. Bárány, H. Cederquist, N. Selberg, and D. C. Lorents, Phys. Rev. A **52**, 3847 (1995).  
[11] U. Thumm, J. Phys. B **28**, 91 (1995).  
[12] F. Chandezon, C. Guet, B. A. Huber, D. Jalabert, M. Maurel, E. Monnard, C. Ristori, and J. C. Rocco, Phys. Rev. Lett. **74**, 3784 (1995).  
[13] C. Guet, X. Biquard, P. Blaise, S. A. Blundell, M. Gross, B. A. Huber, D. Jalabert, M. Maurel, L. Plagne, and J. C. Rocco, Z. Phys. D **40**, 317 (1997).  
[14] F. Martín, P. A. Hervieux, J. Hanssen, M. E. Madjet, and M. F. Politis, Phys. Rev. B (to be published).  
[15] K. J. Børve and J. P. Hansen, Z. Phys. D **25**, 247 (1993).  
[16] M. Madjet, C. Guet, and W. R. Johnson, Phys. Rev. A **51**, 1327 (1995).  
[17] J. F. Reading, Phys. Rev. A **8**, 3262 (1973).  
[18] H. J. Lüdde and R. M. Dreizler, J. Phys. B **18**, 107 (1985).  
[19] N. W. Ashcroft and N. D. Mermin, *Solid State Physics* (W. B. Saunders Co., Philadelphia, 1976).  
[20] C. Bréchnignac, Ph. Cahuzac, F. Carlier, M. de Frutos, and J. Leygnier, Chem. Phys. Lett. **189**, 28 (1992).  
[21] O. Gunnarsson and B. I. Lundqvist, Phys. Rev. B **13**, 4274 (1976).  
[22] J. P. Perdew and A. Zunger, Phys. Rev. B **23**, 5048 (1981).  
[23] J. M. Pacheco and W. Ekardt, Ann. Phys. (Leipzig) **1**, 254 (1992).  
[24] J. M. Pacheco and W. Ekardt, Z. Phys. D **24**, 65 (1992).  
[25] P. Stampfli and K. H. Bennemann, Phys. Rev. A **39**, 1007 (1989).  
[26] M. M. Kappes, M. Schär, U. Röthlisberger, G. Yeretzian, and E. Schumacher, Chem. Phys. Lett. **143**, 251 (1988).  
[27] J. D. Jackson, *Classical Electrodynamics*, 2nd ed. (Wiley, New York, 1962).  
[28] H. J. Lüdde, A. Macías, F. Martín, A. Riera, and J. L. Sanz, J. Phys. B **28**, 4101 (1995).

- [29] R. L. Becker, A. L. Ford, and J. F. Reading, *Phys. Rev. A* **29**, 3111 (1984).
- [30] A. Macías and A. Riera, *Phys. Rep.* **90**, 299 (1982).
- [31] A. Salin, *Comput. Phys. Commun.* **62**, 58 (1991).
- [32] R. Shingal, B. H. Bransden, A. M. Ermolaev, D. R. Flower, C. W. Newby, and C. J. Noble, *J. Phys. B* **19**, 309 (1986).
- [33] R. J. Allan, *J. Phys. B* **19**, 321 (1986).
- [34] J. Lindhard, *K. Dan. Vidensk. Selsk. Mat. Fys. Medd.* **8**, 28 (1954).
- [35] C. Bréchnignac, Ph. Cahuzac, J. Leygnier, and J. Weiner, *J. Chem. Phys.* **90**, 1492 (1989).
- [36] P. A. Hervieux and D. H. E. Gross, *Z. Phys. D* **33**, 295 (1995).